Applied Mathematical Modelling 77 (2020) 724–737

Contents lists available at ScienceDirect

Applied Mathematical Modelling

journal homepage: www.elsevier.com/locate/apm

Completed repeated Richardson extrapolation for compressible fluid flows

Nicholas D.P. da Silva[a,*], Carlos H. Marchi[a], Luciano K. Araki[a], Rafael B. de Rezende Borges[b], Guilherme Bertoldo[c], Chi-Wang Shu[d]

[a] Laboratory of Numerical Experimentation, Department of Mechanical Engineering, Federal University of Paraná, Curitiba, Brazil
[b] Mathematics and Statistics Institute, Rio de Janeiro State University, Rio de Janeiro, Brazil
[c] Department of Physics, Statistics and Mathematics, Federal University of Technology - Paraná, Francisco Beltrão, Brazil
[d] Division of Applied Mathematics, Brown University, Providence, United States of America

ARTICLE INFO

Article history:
Received 11 December 2018
Revised 25 May 2019
Accepted 11 July 2019
Available online 17 July 2019

Keywords:
Richardson extrapolation
Compressible fluid flow
Rayleigh flow
Quasi-one-dimensional flow

ABSTRACT

Richardson extrapolation is a powerful approach for reducing spatial discretization errors and increasing, in this way, the accuracy of the computed solution obtained by use of many numerical methods for solving different scientific and engineering problems. This approach has been used in a variety of computational fluid dynamics problems to reduce numerical errors, but its use has been restricted mainly to the computation of incompressible fluid flows and on grids with coincident nodes. In this work we present a completed repeated Richardson extrapolation (CRRE) procedure for a more generic type of grid not necessarily with coincident nodes, and test it on compressible fluid flows. Three tests are performed for one-dimensional and quasi-one-dimensional Euler equations: (i) Rayleigh flow, (ii) isentropic flow, and (iii) adiabatic flow through a nozzle. The last test involves a normal shock wave. To build a simple solver, these problems are solved by a first-order upwind-type finite difference method as the base scheme. The normal shock wave problem is also solved with a high-order weighted essentially nonoscillatory (WENO) scheme to compare it with the CRRE procedure. The procedure we propose can increase the achieved accuracy and significantly decrease the magnitude of the spatial error in all three tests. Its performance is best demonstrated in the Rayleigh flow test, where the spatial discretization error is reduced by seven orders of magnitude and the achieved accuracy is increased from 0.998 to 6.62 on a grid with 10,240 nodes. Similar performance is observed for isentropic flow, for which the spatial discretization error is reduced by nine orders of magnitude and the achieved accuracy is increased from 0.996 to 6.73 on a grid with 10,240 nodes. Finally, in adiabatic flow with a normal shock wave, the procedure can reduce the spatial discretization error both upstream and downstream of the shock. However, the more expensive high-order WENO scheme results in errors of lower magnitude upstream of the shock and a sharper shock transition for this shocked test case.

* Corresponding author.
E-mail addresses: ndicati@gmail.com (N.D.P. da Silva), rafael.borges@ime.uerj.br (R.B. de Rezende Borges), shu@dam.brown.edu (C.-W. Shu).

https://doi.org/10.1016/j.apm.2019.07.024
0307-904X/

1. Introduction

In fluid mechanics, the set of equations describing an inviscid fluid flow are known as the Euler equations, which constitute a nonlinear hyperbolic system of conservation laws and are a particular case of the Navier–Stokes equations for zero viscosity and thermal conductivity [1]. Although more restrictive than the Navier–Stokes equations, the Euler equations can model compressible fluid flows, or, in other words, high-speed internal and external flows. These equations are very important in modern engineering, but their solution requires the use of numerical methods, and as a consequence, numerical errors arise. The most common approaches in numerical analysis to reduce the numerical error are grid refinement and the use of higher-order numerical schemes, to which Richardson extrapolation (RE) is an alternative.

RE has been used in distinct contexts; for example, step size control [2], error estimation [3], and error reduction. Since the original work of Richardson [4], RE for error reduction has been used repeatedly [5], in a completed manner (CRE) [6], completed with repetition [7], and with Runge–Kutta methods [8], and to compute eigenvalues of the Helmholtz equation [9]. The applications of RE to reduce numerical errors range from simple computational fluid dynamics (CFD) problems to complex ones [10]. There have been two recent modifications of RE to reduce numerical errors. The first one was for secondary variables (e.g., average temperature) and used polynomials to achieve higher accuracy orders [11]. The second modification was made in the CRE procedure to achieve higher accuracy in the entire property field [7].

The original CRE and the last modification mentioned above were intended for grids with coincident nodes, as shown in Fig. 1, where g is the grid level and the refinement ratio (r) between grids is set as 2. The coarse grid ($g = 1$) has nodes coincident with nodes of the fine grid ($g = 2$). A grid with non-coincident nodes is presented in Fig. 2, where we can see that there are no coincident nodes for $r = 2$. Grids with non-coincident nodes *are* used in CFD, notably for finite volume-type methods, although in this article we concentrate on the use of finite difference methods.

In nonlinear hyperbolic systems of conservation laws, the speed of propagation is an important feature. The Euler equations can model subsonic and supersonic flows that depend on the speed of propagation and are subject to the possible appearance of discontinuities, including shocks. Because of this complication, one needs to use robust numerical schemes to solve these conservation laws. For finite difference schemes, one could use simple upwind or upwind-biased first-order methods, such as the Lax–Friedrichs method (see, e.g., [12]). However, such first-order methods are highly dissipative. Higher-order methods can also be used, such as the total variation diminishing scheme or the weighted essentially nonoscillatory (WENO) scheme (see, e.g., [12]). However, these are nonlinear schemes that add extra computational effort and complexity to the solver, and they can suffer from accuracy degeneration in the presence of shocks [13].

The main advantage of the RE procedure is that it increases the accuracy of the spatial discretization and reduces its errors with low computational effort, as reported in [11,14]. Although RE can be used with higher-order base schemes [15], it is more advantageous to use it with lower-order schemes because they are computationally less expensive and are more robust for compressible fluid flows with possible discontinuities in their solution. Since RE (with repetition) and CRE (with and without repetition) have already been developed for incompressible fluid flows and for grids with coincident nodes (see, e.g., [7,11,14]), and since it is more advantageous to use lower-order schemes with RE especially for compressible flows, in this work we present a completed repeated RE (CRRE) procedure for grids with possibly non-coincident nodes, which are often used for compressible flows, and test it with a first-order compressible fluid flow solver as the base scheme. The tests are performed on numerical solutions of one-dimensional (1D) and quasi-one-dimensional (Q1D) Euler equations with steady-state solutions. To solve these equations, we use an explicit first-order upwind-biased finite difference method with Lax–Friedrichs splitting, and an optimal strong-stability-preserving third-order Runge–Kutta method for the time step integration [12] to reach steady states. To assess the performance of the procedure in the presence of shocks, we solve the same shocked problem with the high-order nonlinear WENO-Z scheme [16] for the purpose of comparison.

2. Mathematical model and numerical methods

The conservation law we are interested in has the general form

$$\boldsymbol{U}_t + \boldsymbol{F}(\boldsymbol{U})_x = \boldsymbol{S}(\boldsymbol{U}), \tag{1}$$

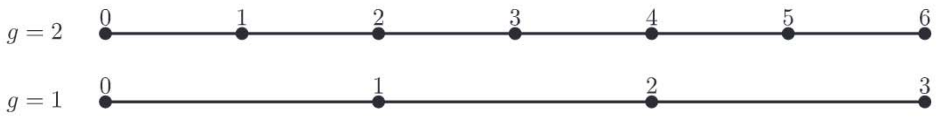

Fig. 1. Grid with coincident nodes.

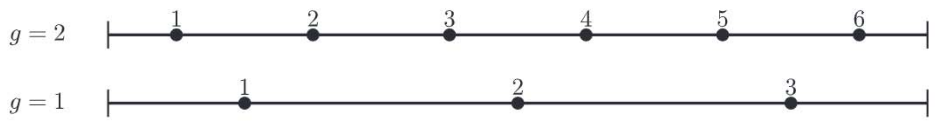

Fig. 2. Grid with non-coincident nodes.

Table 1
Inflow conditions and other parameters for 1D flow.

R (J/(kg K)	286.9	T (K)	400
q (J/kg)	5×10^4	p (MPa)	0.20265
x_l (m)	0	ρ (kg/m^3)	$p/(RT)$
x_r (m)	0.2	v (m/s)	$M\sqrt{\gamma p/\rho}$
M	1.3		

Table 2
Q1D flow parameters.

x_l (m)	0	p_0 (MPa)	0.2
x_r (m)	0.5	T_0 (K)	800
x_{th} (m)	0.25	ρ_0 (kg/m^3)	$p_0/(RT_0)$
r_{th} (m)	0.05	p_e (MPa)	0.101325

where $\boldsymbol{U}$ is the vector of the conservative variables, $\boldsymbol{F}$ is the physical flux, and $\boldsymbol{S}$ is a source term.

The first test for the CRRE procedure is a steady 1D compressible fluid flow. The flow is also known as Rayleigh flow or flow with heat addition. In our case, the inflow is supersonic and heat is being taken to maintain this condition. The conservative variables, flux, and source vectors are

$$\boldsymbol{U} = \begin{bmatrix} \rho \\ \rho v \\ E \end{bmatrix}, \quad \boldsymbol{F}(\boldsymbol{U}) = \begin{bmatrix} \rho v \\ \rho v^2 + p \\ v(E+p) \end{bmatrix} \quad \text{and} \quad \boldsymbol{S}(\boldsymbol{U}) = \begin{bmatrix} 0 \\ 0 \\ \dfrac{-\Delta q \rho v}{h} \end{bmatrix}, \tag{2}$$

where ρ, v, E, p, and h are the density, velocity, total energy, pressure, and discretization partition size, respectively. $\Delta q \equiv q/N$ is the heat taken in each node and q is the total heat per unit mass taken from the flow. The equation of state is given by

$$E = \frac{p}{\gamma - 1} + \frac{\rho v^2}{2}, \tag{3}$$

where $\gamma = 1.4$ is the specific heat ratio for air. One should note that we are using the perfect gas equation of state. The inflow conditions and q are given in Table 1, where R, M, T, x_r, and x_l are the gas constant, Mach number, temperature, the right boundary position, and the left boundary position, respectively.

The Q1D tests involve a steady compressible fluid flow in a convergent–divergent idealized nozzle, whose geometry (cross-sectional area) is computed by

$$A(x) = \pi[(x - \mathrm{xth})^2 + \mathrm{rth}]^2, \tag{4}$$

where xth and rth are the position and the radius of the throat, respectively.

Depending on the inflow and outflow conditions, a smooth (isentropic) or discontinuous (adiabatic) solution may be obtained. The conservative variables and flux vectors are the same as in the 1D test. The source term is

$$\boldsymbol{S}(\boldsymbol{U}) = -\frac{A_x}{A}\begin{bmatrix} \rho u \\ \rho u^2 \\ u(E+p) \end{bmatrix}. \tag{5}$$

The flow parameters are presented in Table 2, where the subscript 0 denotes the total or stagnation properties and p_e is the pressure at the nozzle exit. If a certain p_e is imposed at the outflow boundary, a normal shock wave can stand at some position in the divergent region of the nozzle (more details can be found in [17]).

The domain is discretized as follows (see Fig. 2):

$$x_i = x_l + h(i - 1/2), \quad 1 \le i \le N, \quad \text{and} \quad h = (x_r - x_l)/N,$$

where N is the number of nodes.

For the finite difference method, we approximate (1) as

$$\frac{d}{dt}\boldsymbol{U}_i = -\frac{1}{h}(\hat{\boldsymbol{F}}_{i+1/2} - \hat{\boldsymbol{F}}_{i-1/2}) + \boldsymbol{S}(\boldsymbol{U}_i), \tag{6}$$

where $\hat{\boldsymbol{F}}$ is the numerical flux. We refer to [12] for the first-order Lax–Friedrichs flux and to [16] for the higher-order WENO-Z flux. The time stepping is implemented by a strong-stability-preserving third-order Runge–Kutta method [12] to integrate (6) in time:

$$\begin{aligned} \boldsymbol{U}^{(1)} &= \boldsymbol{U}^n + k\boldsymbol{L}(\boldsymbol{U}^n), \\ \boldsymbol{U}^{(2)} &= \frac{3\boldsymbol{U}^n + \boldsymbol{U}^{(1)} + k\boldsymbol{L}(\boldsymbol{U}^{(1)})}{4}, \\ \boldsymbol{U}^{n+1} &= \frac{\boldsymbol{U}^n + 2\boldsymbol{U}^{(2)} + 2k\boldsymbol{L}(\boldsymbol{U}^{(2)})}{3}, \end{aligned} \tag{7}$$

where $\boldsymbol{L}(\boldsymbol{U})$ is the spatial discretization operator. For stability, we use the time step k as

$$k = \frac{h\,\mathrm{CFL}}{\alpha}, \tag{8}$$

where $\mathrm{CFL} = 0.5$, $\alpha = \max_{\boldsymbol{U}} \max_{1\le j\le 3} |\lambda_j(\boldsymbol{U})|$, and $\lambda_j(\boldsymbol{U})$ are the eigenvalues of the Jacobian $f'(\boldsymbol{U})$. This time step is valid for the upwind, and the required time step for the WENO-Z scheme is

$$k = \min\left(\frac{h\,\mathrm{CFL}}{\alpha}, h^{5/3}\right). \tag{9}$$

For the boundary conditions, we use the inverse Lax–Wendroff procedure [18,19] to maintain higher order at the boundaries.

With regard to Rayleigh flow, we use the analytical solution as the initial condition (see [17] for details of the analytical solution). Note that, to the numerical scheme, this is *not* a solution; hence, we need to march in time to reach the steady state. The time integration will be stopped when the residue reaches machine epsilon (round-off error).

Since the inflow is supersonic, we impose all three components of the solution u_1, u_2, and u_3 at the inflow boundary, and extrapolate all of them to the ghost nodes via Taylor expansion [18]. Because our base scheme is first-order accurate, the values at the ghost node are the same as at the boundary.

The outflow is also supersonic, and we extrapolate the characteristic variables to get $\boldsymbol{U}$ at the boundary and then at the ghost node (see [18] for details of the inverse Lax–Wendroff procedure). Although our base scheme is first-order accurate, our numerical tests have shown that a higher-order extrapolation (e.g., fifth-order accurate) is needed to maintain the designed high-order accuracy of the CRRE procedure at the outflow boundary.

For Q1D flow, we again use the exact solution as the initial condition (see [17] for details of the exact solution for the Q1D flow) and the time integration is stopped when the residue reaches machine epsilon (round-off error).

The inflow is subsonic for both isentropic flow and adiabatic flow. Therefore, we impose two conservative variables and extrapolate one characteristic variable. With the exact solution, we impose u_1 and u_2 and extrapolate the first characteristic variable v_1 corresponding to the negative eigenvalue at the left boundary, then extrapolate $\boldsymbol{U}$ to the ghost node. As before, even though our scheme is first-order accurate, we still need to use a high-order (we use a fifth-order) extrapolation to maintain the designed high-order accuracy of the CRRE procedure.

Finally, for the last test, which consists of a Q1D adiabatic flow with a normal shock wave, the outflow is subsonic and we impose one conservative variable and extrapolate two characteristic variables. With the exact solution, we impose u_1 and extrapolate the two characteristic variables v_2 and v_3 corresponding to the two positive eigenvalues at the right boundary, and then extrapolate $\boldsymbol{U}$ to the ghost node. Because the first three grids are very coarse and the scheme is first-order accurate, the shock may cause oscillation problems near the outflow boundary. To avoid these oscillations, we reduce the extrapolation order in the coarse grids. The oscillation problems could also be avoided by use of a WENO-type extrapolation [18,19]. However, such nonlinear WENO-type extrapolation seems to cause order reduction with the CRRE procedure. In isentropic flow, the outflow is supersonic and we treat it in a similar way as in the 1D test.

Once the numerical solutions have been obtained by the numerical methods presented in this section, their spatial accuracy can be increased by application of the RE procedure. The application leads to additional computational effort but better accuracy properties will compensate for the additional computations. Furthermore, the computational effort added by the RE is negligible when compared with the effort needed for computation on finer grids [11,14]. The RE procedure we propose is presented in Section 4.3.

3. Verification

As stated in [20], verification assesses the code and solution correctness and involves error evaluation and estimation in a systematic grid refinement. This analysis is done by means of the error itself, numerical error estimate, and accuracy orders. The numerical error can be the difference between the exact solution and the numerical solution, if the former is available, or the difference between the numerical solutions from different meshes. To get reliable results, the achieved accuracy should approach the asymptotic order (p_0), ideally monotonically, in more than three grids [20,21]. The asymptotic order p_0 depends on the numerical scheme itself and the regularity of the exact solution, which is obtained a priori, regardless of the numerical solution [21,22]. As we will be considering problems with known analytical or exact solutions, these will be used to compute the numerical errors and achieved accuracy.

The error and accuracy analysis will be performed in the entire property field (e.g., density) of the steady converged solution by means of the L^1 norm; that is,

$$\|E_g^m\|_{L^1} = \frac{1}{N}\sum_{i=1}^{N} |E_{g,i}^m| \tag{10}$$

with

$$E_{g,i}^m = \tilde{u}(x_i) - u_{g,i}^m, \tag{11}$$

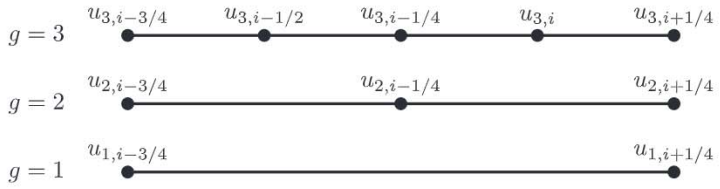

Fig. 3. Grid with coincident nodes in three levels and $r = 2$.

where u is the steady converged numerical solution, $\tilde{u}$ is the analytical or exact solution, the superscript m refers to the CRE level, and the subscripts g and i refer to the grid level and the node position, respectively. One should note that $m = 0$ is the numerical solution without any CRE. Also, to avoid confusion, the numerical solution without CRE will not have a superscript.

The achieved accuracy can be computed as

$$p_{E_g^m} = \frac{\log_{10}(\|E_{g-1}^m\|_{L^1} / \|E_g^m\|_{L^1})}{\log_{10}(r)}. \tag{12}$$

The achieved accuracy may not be (and often is not) an integer.

4. Richardson extrapolation

4.1. Completed Richardson extrapolation

The RE is based on the assumption that discrete solutions have a series representation in terms of the discretization partition size h. For instance [22],

$$u = \tilde{u}(x) + c_1 h^{p_0} + c_2 h^{p_1} + c_3 h^{p_2} + \mathcal{O}(h^{p_3}), \tag{13}$$

where $p_0 < p_1 < p_2 < \ldots$ are the true orders with RE, which depend on the numerical scheme and approximations. In our case, the true orders for the first-order upwind base scheme are $1, 2, 3, \ldots$ and the true orders for the WENO-Z scheme are $5, 6, 7, \ldots$.

As the grid is refined ($h \to 0$), the first term of h dominates and the numerical solution at the vth level can be expressed as

$$u = u_\infty + c_v h^{p_v}, \tag{14}$$

where u_∞, called the *extrapolated solution*, is an approximation to the analytical solution. It is a better approximation than u, as the order of accuracy is p_{v+1}, which is bigger than p_v.

If one has the numerical solution on two distinct grids, (14) can be written for these two grids and combined to compute u_∞ as

$$u_\infty = u_g + \frac{u_g - u_{g-1}}{r^{p_v} - 1}. \tag{15}$$

From the RE, one can also obtain the Richardson error estimate U_{ri},

$$U_{ri} = u_\infty - u_g. \tag{16}$$

Roache and Knupp [6] devised a method based on (15) for the entire property field called *CRE* using a grid with coincident nodes. Since the grid has coincident nodes, they proposed that

$$u_\infty = u_g + C_i, \tag{17}$$

with a correction

$$C_i = \frac{u_g - u_{g-1}}{r^{p_v} - 1}, \tag{18}$$

for the coincident nodes (e.g., see nodes $u_{1,i-3/4}$, $u_{2,i-3/4}$, $u_{1,i+1/4}$, and $u_{2,i+1/4}$ in Fig. 3) and

$$C_i = \frac{C_{i+1} + C_{i-1}}{2} \tag{19}$$

for the other nodes (see node $u_{2,i-1/4}$ in Fig. 3).

4.2. Assessment of completed Richardson extrapolation with repetition

Let us consider the CRE with repetition. Fig. 3 shows three different grid levels with $r = 2$ and the numerical solution without CRE. The goal is to assess the accuracy at the node i with two levels of CRE.

The error for a first-order scheme at a generic node (e.g., $i - 3/4$, $i - 1/4$, i, and $i + 1/4$) can be assessed through the following Taylor expansions ($h_3 = h_2/2 = h_1/4 = h/4$, since $r = 2$):

$$u_{3,i} - \tilde{u}(x_i) = c_{1,i}\frac{h}{4} + c_{2,i}\left(\frac{h}{4}\right)^2 + c_{3,i}\left(\frac{h}{4}\right)^3 + \mathcal{O}(h^4), \tag{20}$$

$$u_{2,i} - \tilde{u}(x_i) = c_{1,i}\frac{h}{2} + c_{2,i}\left(\frac{h}{2}\right)^2 + c_{3,i}\left(\frac{h}{2}\right)^3 + \mathcal{O}(h^4), \tag{21}$$

$$u_{1,i} - \tilde{u}(x_i) = c_{1,i}h + c_{2,i}h^2 + c_{3,i}h^3 + \mathcal{O}(h^4). \tag{22}$$

For the first CRE level, we substitute (21) and (22) in (17) regarding the node positions. Hence,

$$u^1_{2,i-3/4} - \tilde{u}(x_{i-3/4}) = -c_{2,i-3/4}\frac{h^2}{2} - 3c_{3,i-3/4}\frac{h^3}{4} + \mathcal{O}(h^4), \tag{23}$$

$$u^1_{2,i+1/4} - \tilde{u}(x_{i+1/4}) = -c_{2,i+1/4}\frac{h^2}{2} - 3c_{3,i+1/4}\frac{h^3}{4} + \mathcal{O}(h^4). \tag{24}$$

Since $c_{1,i}$ is a function of x and assuming it is smooth, one can expand $c_{1,i-3/4}$ and $c_{1,i+1/4}$ to get

$$c_{1,i-3/4} = c_{1,i-1/4} - c^{(1)}_{1,i-1/4}\frac{h}{2} + c^{(2)}_{1,i-1/4}\frac{h^2}{8} + \mathcal{O}(h^3), \tag{25}$$

$$c_{1,i+1/4} = c_{1,i-1/4} + c^{(1)}_{1,i-1/4}\frac{h}{2} + c^{(2)}_{1,i-1/4}\frac{h^2}{8} + \mathcal{O}(h^3). \tag{26}$$

Using the same idea for the other terms, we can write

$$u^1_{2,i-1/4} - \tilde{u}(x_{i-1/4}) = -c_{2,i-1/4}\frac{h^2}{2} - (c^{(2)}_{1,i-1/4} + 12c_{3,i-1/4})\frac{h^3}{16} + \mathcal{O}(h^4), \tag{27}$$

$$u^1_{3,i-1/4} - \tilde{u}(x_{i-1/4}) = -c_{2,i-1/4}\frac{h^2}{8} - 3c_{3,i-1/4}\frac{h^3}{32} + \mathcal{O}(h^4), \tag{28}$$

$$u^1_{3,i+1/4} - \tilde{u}(x_{i+1/4}) = -c_{2,i+1/4}\frac{h^2}{8} - 3c_{3,i+1/4}\frac{h^3}{32} + \mathcal{O}(h^4), \tag{29}$$

$$u^1_{3,i} - \tilde{u}(x_i) = -c_{2,i}\frac{h^2}{8} - \left(c^{(2)}_{1,i} + 12c_{3,i}\right)\frac{h^3}{128} + \mathcal{O}(h^4). \tag{30}$$

For the second CRE level

$$u^2_{3,i-1/4} - \tilde{u}(x_{i-1/4}) = (c^{(2)}_{1,i-1/4} + 6c_{3,i-1/4})\frac{h^3}{48} + \mathcal{O}(h^4), \tag{31}$$

$$u^2_{3,i+1/4} - \tilde{u}(x_{i+1/4}) = c_{3,i+1/4}\frac{h^3}{8} + \mathcal{O}(h^4), \tag{32}$$

$$u^2_{3,i} - \tilde{u}(x_i) = c_{2,i}\frac{h^2}{4} + (c^{(2)}_{1,i} + 72c_{3,i})\frac{h^3}{128} + \mathcal{O}(h^4), \tag{33}$$

where we can see that the accuracy is 2 at $g = 3$, the second level of CRE, and node i. This is a problem because after the first level the CRE will not be able to eliminate this second-order error term.

C_i for non-coincident nodes are second-order approximations, and one possible remedy for the order limitation would be to use a higher-order computation of C_i. However, this must be done for each non-coincident C_i at every CRE level.

A cheaper remedy to achieve higher orders with CRE and repetition would be to use (15) at the coincident nodes only (e.g., nodes $i - 3/4$ and $i + 1/4$ in Fig. 3) and then obtain higher-order approximations at the other nodes with a suitable interpolation. Unfortunately, this cannot be done for grids with only non-coincident nodes. Therefore, a different approach must be devised to increase the accuracy of the solution for grids of this type.

4.3. Completed repeated Richardson extrapolation

As a first approach, to increase the accuracy for grids with non-coincident nodes, one could combine three nodes and compute a correction in a similar way to that in the original CRE. However, a fixed-order correction would impose a limit

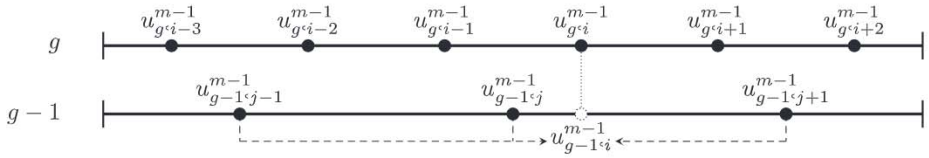

Fig. 4. Extrapolation between two grid levels.

Table 3
Extrapolations to u.

Grid level (g)	CRE level (m)				
	0	1	2	3	4
1	$u_{1,i}$	–	–	–	–
2	$u_{2,i}$	$u^1_{2,i}$	–	–	–
3	$u_{3,i}$	$u^1_{3,i}$	$u^2_{3,i}$	–	–
4	$u_{4,i}$	$u^1_{4,i}$	$u^2_{4,i}$	$u^3_{4,i}$	–
5	$u_{5,i}$	$u^1_{5,i}$	$u^2_{5,i}$	$u^3_{5,i}$	$u^4_{5,i}$
				CRRE	

on the order of the procedure. Another approach would be the combination of more than three nodes to achieve higher orders. Nevertheless, higher orders demand a large number of nodes and, therefore, a large system to solve. This system may not be solvable. The easiest, but perhaps not the cheapest, approach is to use repetition.

First, we write

$$u^m_{g,i} = u^{m-1}_{g,i} + \frac{u^{m-1}_{g,i} - u^{m-1}_{g-1,i}}{r^{p_{m-1}} - 1}, \text{ with } m = 1, \ldots, G-1 \text{ and } m < g, \tag{34}$$

where G is the number of grids. The first level ($m = 1$) of CRE depends on the numerical solution ($m = 0$).

To compute the CRE at level m, one needs an equivalent node in the coarse grid ($g-1$). That is, one needs $u^{m-1}_{g,i}$ and an equivalent $u^{m-1}_{g-1,i}$. This can be done with a Newton polynomial $p_d(x)$ of degree $d = l + r = p_{G-1} - 1$ with l nodes to the left and r nodes to right of i, satisfying $p_d(x_j) = u^{m-1}_{g-1,j}$ with $j = i-l, \ldots, i+r$ and $i = 1, \ldots, N$, as shown in Fig. 4.

If we have $G = 10$ grid levels, then it is possible to compute $G - 1 = 9$ CRE levels. If the true orders are $1, 2, 3, \ldots$, it is expected we can reach tenth order with CRRE ($p_9 = 10$). A ninth-degree polynomial is required because experiments have shown that CRE cannot remove lower-order terms inserted by the polynomial.

Once all fine grid nodes have equivalent nodes in the coarse grid, the extrapolation can be computed with (34). CRRE is a recursive application of CRE and it is summarized in Table 3.

The algorithm for computing the CRRE in smooth solutions at level m is summarized next. For $g = m+1, \ldots, G$, proceed as follows:

1. Obtain an equivalent node in the coarse mesh $\{u^{m-1}_{g-1,i}\}$ with a Newton polynomial of degree $p_{G-1} - 1$.
2. Compute the CRE with (34).

The compressible fluid flow is subject to discontinuities and shocks, which are challenging issues for numerical methods. One of the most popular numerical schemes used to capture shocks in conservation laws, such as the Euler equations, is the WENO scheme [12,16]. Through the weighted combination of approximations in different substencils, this scheme can maintain higher order sufficiently far from the shock. Considering this, we propose use of the WENO idea with CRRE to reduce the error in solutions with shocks.

To reduce spatial discretization error, the CRRE must be computed sufficiently far from the shock. To accomplish that, we use the WENO smoothness indicator idea and the Richardson error estimate as a predictor/corrector step, computed as

$$U^m_{rig} = \frac{u^{m-1}_{g,i} - u^{m-1}_{g-1,i}}{r^{p_{m-1}} - 1}. \tag{35}$$

The CRRE smoothness indicator is

$$P_i = \frac{\beta_{g,i}}{\beta_{f,i} + \epsilon}, \tag{36}$$

where $\epsilon = 10^{-16}$ to avoid division by zero. Both $\beta_{f,i}$ and $\beta_{g,i}$ are computed through the following formula [12]:

$$\beta_{v,i} = \sum_j^4 h^{2j-1} \left(\frac{d^j \hat{F}_{v,i}}{dx^j} \right)^2, \qquad v = f, g, \tag{37}$$

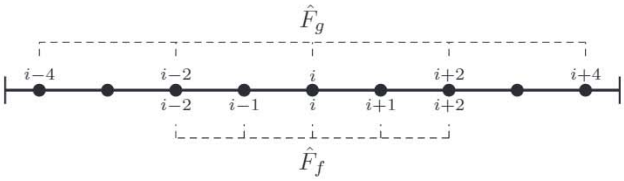

Fig. 5. Example of stencils for $\hat{F}_{g,i}$ and $\hat{F}_{f,i}$.

where $F_{f,i}$ and $F_{g,i}$ are the fourth-degree polynomial interpolations at a finer and a coarser stencil, respectively, around x_i, as shown in Fig. 5.

The value of $\beta_{v,i}$ is of $\mathcal{O}(h^2)$ if $\hat{F}$ is smooth in the stencil v and it is of $\mathcal{O}(1)$ otherwise [23]. Suppose that $\hat{F}$ is smooth in the whole coarse stencil g (which includes the finer stencil f). Since the spatial step in g is twice as large as in f, we have

$$\beta_{f,i} = \mathcal{O}(h^2), \quad \beta_{g,i} = \mathcal{O}((2h)^2) \qquad \therefore \qquad P_i \approx 4.$$

However, if $\hat{F}$ is not smooth in g but is smooth in f, by (36) P_i should be larger than 4. In our experiments, the solution can be assumed to be smooth if

$$P_i \leq 2 + 2^{1+1/p_v^2}. \tag{38}$$

Even with the restriction imposed by (38), the CRRE could be computed in a node with high-magnitude errors. To avoid that, we compute the CRRE in nodes where (38) is satisfied and the Richardson error estimate is lower than in the previous CRE level. Of course, when $m = 0$, there is no error estimate. Therefore, we set U_{ri}^0 as an arbitrary big value.

The algorithm for computing the CRRE at level m in solutions with shocks and for $g = G, \ldots, m+1$ is as follows:

1. Compute P_i in every node and use (38) to determine in which nodes the solution is smooth.
2. Find the beginning (b) and the ending (e) of the nonsmooth region.
3. For $i = 1, \ldots, N$ proceed as follows:
   a. If i is between b and e, use the previous-level value ($u_{g,i}^m = u_{g,i}^{m-1}$).
   b. Otherwise, obtain an equivalent node in the coarse mesh ($u_{g-1,i}^{m-1}$) with a Newton polynomial of degree $p_{G-1} - 1$, avoiding nodes inside the nonsmooth region.
      i. Compute the CRE with (34).
      ii. Compute U_{rig}^m.
      iii. If $|U_{rig}^m| > |U_{rig}^{m-1}|$, use the previous-level value ($u_{g,i}^m = u_{g,i}^{m-1}$).

5. Results

Our interest is to test our method and to assess its performance in increasing the order of the spatial discretization error in compressible fluid flow solutions. In all cases, the spatial discretization error is close to the double-precision machine epsilon (round-off error), and to avoid round-off issues, we use quadruple-precision computing. With quadruple precision, the computational time is greatly increased. To compute solutions more quickly, we use better initial estimates and parallel computing. One of the most precise initial estimates is the analytical solution (which is not the solution to the numerical scheme, and hence time marching is still needed to reach a numerical steady state). However, before computing the solutions, we performed a convergence analysis for more generic initial estimates.

For the 1D problem, we used the inflow values in the entire domain as the initial estimate. For the Q1D isentropic flow, we used a linear distribution from 0 at the left boundary to 2 at the right boundary for the Mach number as an initial estimate. Then we computed the density, velocity, and pressure with the gas dynamics equations and the stagnation properties (shown in Table 2). Finally, for the Q1D flow with normal shock, we used a linear distribution from 0 at the left boundary to 1 at the nozzle throat and another linear distribution from 1 at the nozzle throat to 0 at the right boundary for the Mach number as an initial estimate. The density, velocity, and pressure were computed in a similar way as for isentropic flow.

The convergence analysis was performed on a grid with 640 nodes and is based on the average residue

$$Re = \sum_{i=1}^{N} \frac{|\rho_i^{n+1} - \rho_i^n| + |[\rho v]_i^{n+1} - [\rho v]_i^n| + |E_i^{n+1} - E_i^n|}{kN}, \tag{39}$$

where n and $n+1$ are time step indices. The results are shown in Fig. 6, where one can see that the average residue settles down in all cases, except for the Q1D flow with a normal shock and the WENO-Z scheme. This can happen with WENO schemes, as pointed out in [24]. Furthermore, the residue is greater than the quadruple-precision machine epsilon (round-off error) because of the magnitude of the third $\boldsymbol{U}$ component and k in the denominator. We do not present the verification for these initial estimates because the analysis is the same as in the next sections.

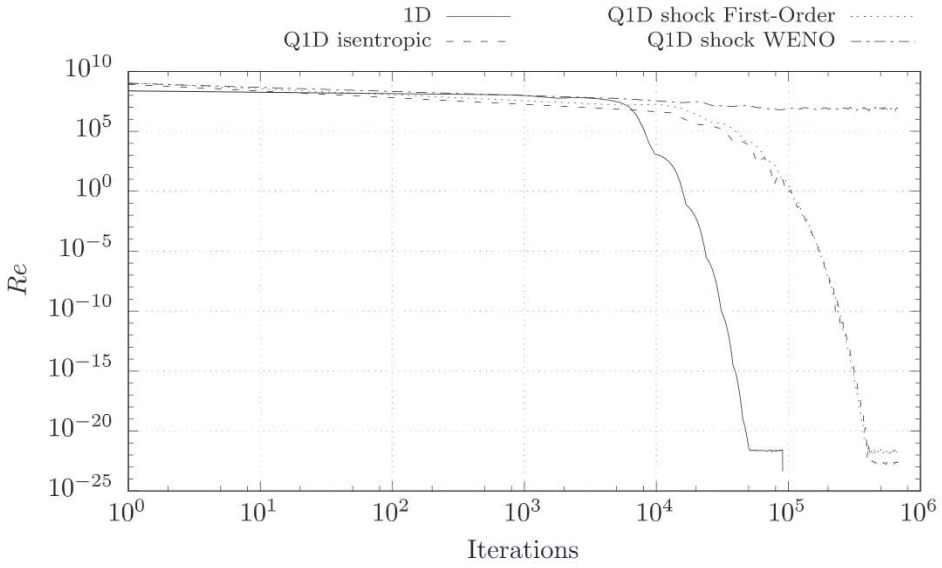

Fig. 6. Average residue for generic initial estimates.

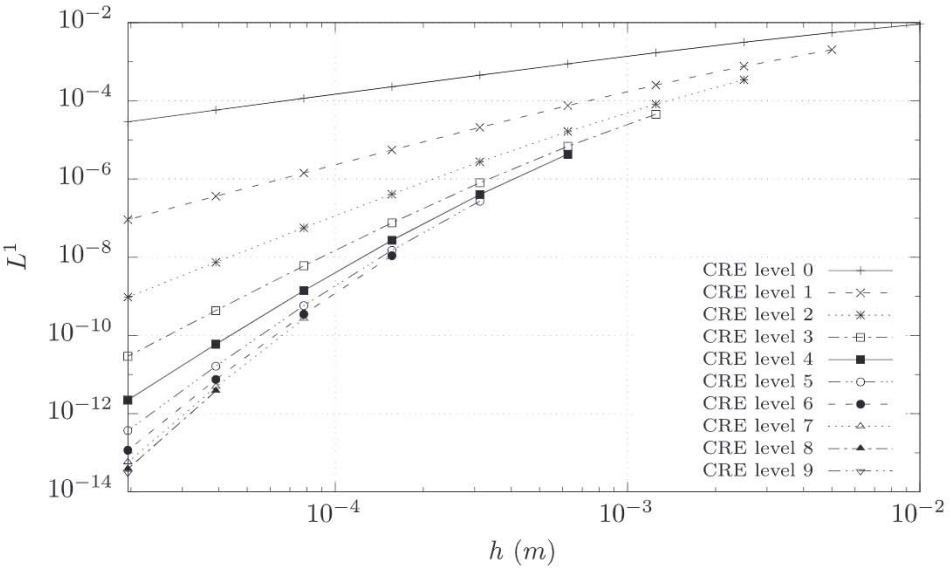

Fig. 7. L^1 norm of ρ at each grid and CRE level for 1D Euler flow.

5.1. One-dimensional Euler equations

The L^1 norm of the error and its achieved accuracy for the density are presented in Figs. 7 and 8, and in Table 4, where we can see the optimal performance of CRRE in increasing the achieved accuracy of the spatial discretization. The results for the other conservative variables are not shown because they are qualitatively similar.

5.2. Quasi-one-dimensional Euler equations

The L^1 norm of the error and its achieved accuracy for the density and isentropic flow are presented in Figs. 9 and 10, and in Table 5, where the performance is seen to be less than in the previous case as not all orders are converging monotonically from the first grid level. However, we can see that the L^1 norm and its achieved accuracy are stabilizing. This nonmonotone behavior could be due to the CRE overestimating or underestimating the error. For instance, the second grid level of the fourth CRE level has a smaller error than expected. The results for the other conservative variables are not shown because they are qualitatively similar.

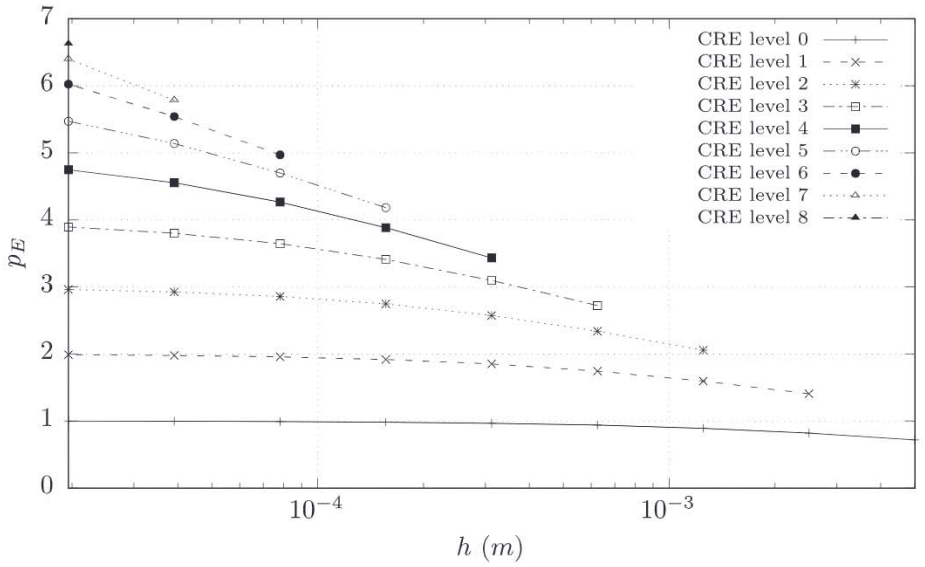

Fig. 8. p_E of ρ at each grid and CRE level for 1D Euler flow.

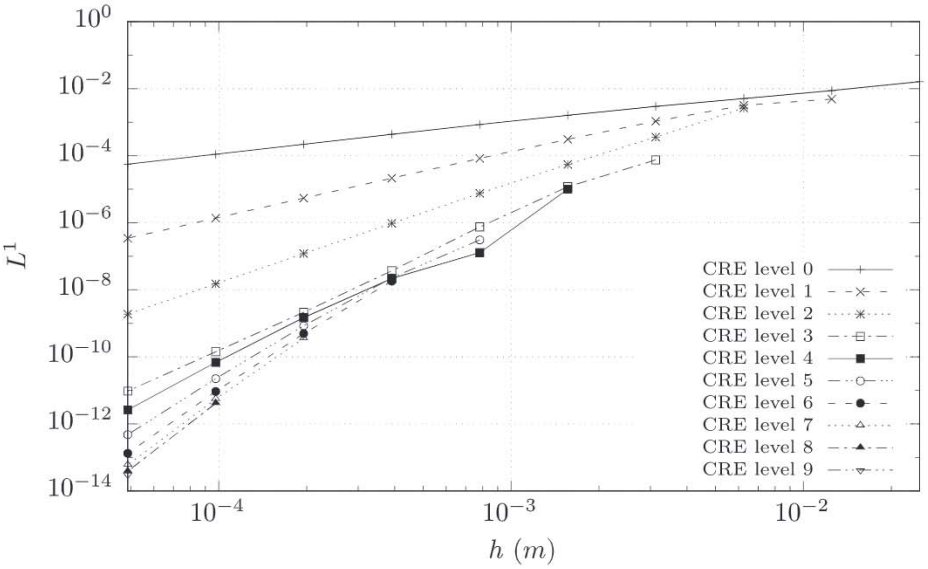

Fig. 9. L^1 norm of ρ at each grid and CRE level for Q1D isentropic flow.

Table 4
Orders and norms of ρ for 1D Euler flow.

Node quantity	Upwind		CRRE	
	L^1 norm	Order	L^1 norm	Order
20	9.15×10^{-3}	–	–	–
40	5.57×10^{-3}	0.717	2.03×10^{-3}	–
80	3.16×10^{-3}	0.819	3.45×10^{-4}	1.41
160	1.70×10^{-3}	0.891	4.54×10^{-5}	2.06
320	8.87×10^{-4}	0.939	4.31×10^{-6}	2.72
640	4.54×10^{-4}	0.967	2.73×10^{-7}	3.43
1280	2.30×10^{-4}	0.983	1.10×10^{-8}	4.18
2560	1.16×10^{-4}	0.991	2.66×10^{-10}	4.97
5120	5.79×10^{-5}	0.995	3.80×10^{-12}	5.79
10240	2.90×10^{-5}	0.998	3.11×10^{-14}	6.62

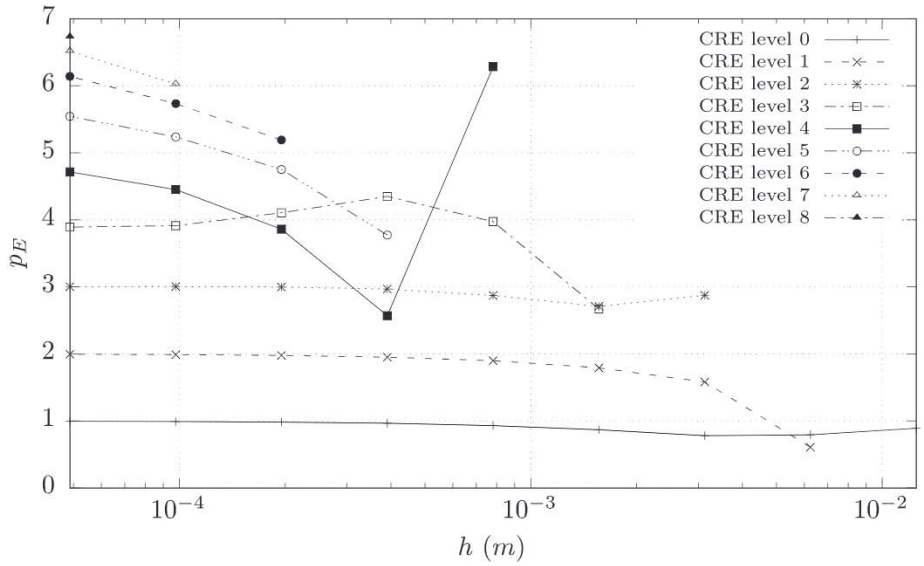

Fig. 10. p_E of ρ error at each grid and CRE level for Q1D isentropic flow.

Table 5
Orders and norms of ρ for Q1D isentropic flow.

Node quantity	Upwind		CRRE	
	L^1 norm	Order	L^1 norm	Order
20	1.63×10^{-2}	–	–	–
40	8.79×10^{-3}	0.890	4.87×10^{-3}	–
80	5.07×10^{-3}	0.794	2.63×10^{-4}	0.609
160	2.95×10^{-3}	0.781	7.49×10^{-5}	2.87
320	1.62×10^{-3}	0.869	9.98×10^{-6}	2.67
640	8.48×10^{-4}	0.931	3.09×10^{-7}	6.28
1280	4.35×10^{-4}	0.965	1.80×10^{-8}	3.77
2560	2.20×10^{-4}	0.982	3.56×10^{-10}	5.19
5120	1.11×10^{-4}	0.991	4.10×10^{-12}	6.02
10240	5.55×10^{-5}	0.996	3.07×10^{-14}	6.73

For the flow with a normal shock wave, it is not convenient to use (10) to compute the L^1 norm because the error behavior is nonmonotone in the shock region. Also, the region downstream of the shock is subject to error degradation from the shock [13]. This does not happen with the region upstream of the shock because of the flow type (i.e., the flow is supersonic and the information cannot propagate upstream of the shock). Therefore, we compute the L^1 norm in the smooth regions of the solution, identified in the same way as in the CRRE procedure. In this test, we also compute the shock problem with the WENO-Z method. The boundary treatment is the same as in the upwind scheme with the exception that we use WENO-type extrapolation [18,19] at the right boundary and that more ghost nodes are needed.

First, we present the solution field and the error at every node for the Mach number and a grid with 5120 nodes in Figs. 11 and 12. The Mach number is computed as

$$M = \frac{v}{\sqrt{\gamma p/\rho}}. \tag{40}$$

In Figs. 11 and 12 the shock transition is sharper for the WENO-Z scheme than for the upwind scheme and the CRRE, and the WENO-Z accuracy degenerates downstream of the shock. Also, despite a higher magnitude for the errors, the CRRE procedure can reduce the error both upstream and downstream of the shock. The accuracy loss for the WENO-Z scheme is a common behavior of higher-order nonlinear methods [13].

The L^1 norm and its achieved accuracy for the Mach number for Q1D flow with a normal shock wave are summarized in Table 6. In this analysis, the WENO-Z error magnitude and order limitation are both due to the loss of accuracy downstream of the shock. To compare the CRRE and the WENO-Z scheme, the L^1 norm and its achieved accuracy are presented only upstream of the shock in Table 7, where one can see that the WENO-Z scheme has lower error magnitude. Because of the shock region, it is difficult to draw conclusions about the convergence order. However, in both cases, the error is being reduced.

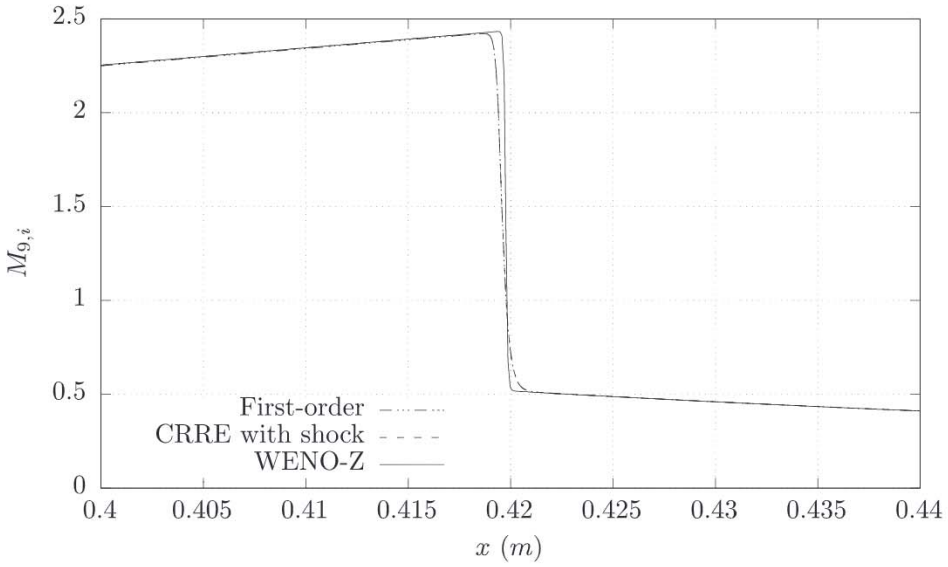

Fig. 11. Mach number, magnified in the shock region, for Q1D flow with a normal shock wave and a grid with 5120 nodes.

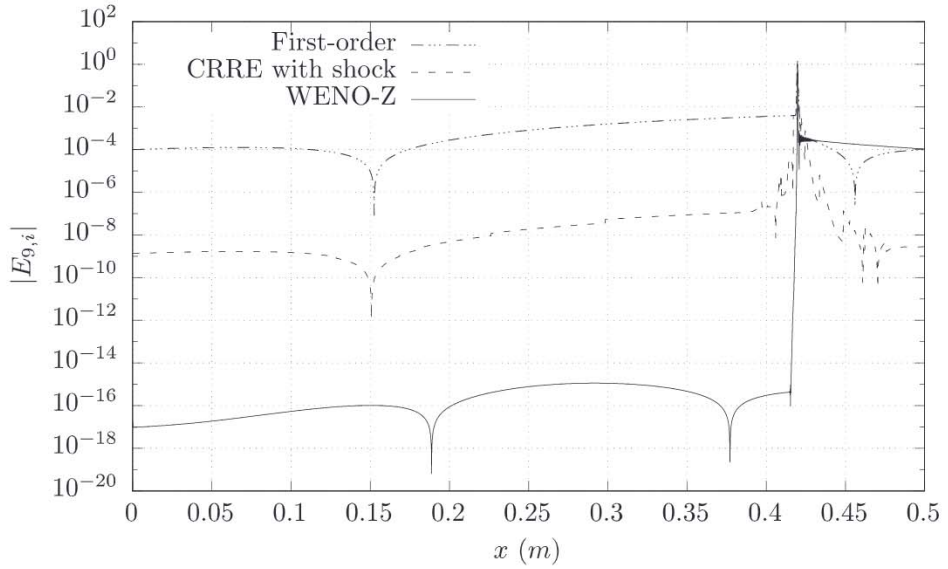

Fig. 12. The absolute value of the error for the Mach number at each node for Q1D flow with a normal shock wave and a grid with 5120 nodes.

Table 6
Orders and norms for the Mach number computed in the smooth regions of the solution for Q1D flow with a normal shock wave.

Node quantity	WENO-Z scheme		CRRE with shock	
	L^1 norm	Order	L^1 norm	Order
20	8.38×10^{-2}	–	–	–
40	1.32×10^{-2}	2.67	1.51×10^{-1}	–
80	1.56×10^{-2}	−0.24	3.54×10^{-2}	2.07
160	6.00×10^{-3}	1.37	9.27×10^{-3}	1.92
320	1.73×10^{-3}	1.80	1.53×10^{-3}	2.60
640	7.80×10^{-4}	1.15	1.01×10^{-4}	3.93
1280	1.04×10^{-5}	6.24	3.69×10^{-6}	4.77
2560	4.64×10^{-6}	1.16	4.50×10^{-7}	3.04
5120	2.47×10^{-6}	0.91	2.60×10^{-8}	4.11

Table 7
Orders and norms for the Mach number computed upstream of the shock.

Node quantity	WENO-Z scheme		CRRE with shock	
	L^1 norm	Order	L^1 norm	Order
20	8.38×10^{-2}	–	–	–
40	1.30×10^{-2}	2.69	1.04×10^{-1}	–
80	1.58×10^{-2}	−0.28	3.92×10^{-2}	1.37
160	6.12×10^{-3}	1.36	9.44×10^{-3}	2.05
320	1.73×10^{-3}	1.83	1.45×10^{-3}	2.70
640	6.25×10^{-4}	1.46	6.08×10^{-5}	4.58
1280	7.56×10^{-7}	9.69	1.73×10^{-6}	5.14
2560	4.44×10^{-10}	10.7	3.43×10^{-7}	2.34
5120	5.11×10^{-12}	6.44	2.81×10^{-8}	3.61

The negative order values, shown in Tables 6 and 7 for the WENO-Z scheme, occur because of the smooth region detection. Clearly, this procedure underestimates the shock region for the WENO-Z solution.

6. Concluding remarks

The classical CRE procedure and its modifications were developed mostly for incompressible fluid flows and for grids with coincident nodes. Nonetheless, it is also very common to solve CFD problems on grids with non-coincident nodes, and compressible fluid flows play an important role in modern CFD. Since it is more advantageous to use RE with lower-order schemes for such cases, we built simple compressible fluid flow solvers to test our CRRE procedure.

We have shown that:

(1) The original CRE procedure is not suitable for repetition, and we proposed a remedy for this situation for grids with coincident nodes. Instead of testing this, we proposed and tested a general CRRE procedure based on interpolation from coarse to fine grid nodes at each level of CRE, which is suitable for compressible fluid flows.
(2) The CRRE procedure was successfully tested in Rayleigh flow, where one can observe the optimal CRRE performance. The error was reduced by seven orders of magnitude and the achieved accuracy was increased from 0.998 to 6.62 on a grid with 10,240 nodes.
(3) For isentropic flow, the performance is less optimal in the sense that the achieved accuracy does not always increase monotonically. However, the error was reduced by nine orders of magnitude and the achieved accuracy was increased from 0.996 to 6.73.
(4) In adiabatic flow with a normal shock wave, CRRE reduced the errors both downstream and upstream of the shock. However, the high-order WENO-Z scheme resulted in errors with smaller magnitude upstream of the shock and a sharper shock transition.

The CRRE procedure works well for compressible fluid flows without shock waves by increasing the achieved accuracy of the spatial discretization and reducing its error significantly. Although the CRRE procedure can also work with shocks, it resulted in errors with higher magnitude and a smoother shock transition than the high-order WENO-Z scheme. Further study is needed to improve the performance of the CRRE procedure for shocked solutions.

We plan to investigate a less expensive treatment for boundary conditions while still maintaining the accuracy of the CRRE procedure, a CRRE procedure with more general equations, including transient problems, and improvement of the CRRE procedure with discontinuous solutions.

Acknowledgments

The authors acknowledge the UNIESPAÇO program of the Brazilian Space Agency (AEB) and the Conselho Nacional de Desenvolvimento Científico e Tecnológico (CNPq), Brazil, for physical and financial support given for this work, and the support of Brown University for facilitating visits between the authors. This study was financed in part by the Coordenação de Aperfeiçoamento de Pessoal de Nível Superior (CAPES), Brazil, Finance Code 001. Nicholas D.P. da Silva thanks Intel for providing a student license of its Fortran compiler. Carlos H. Marchi is supported by a CNPq scholarship. The authors also thank the journal editors and reviewers for their suggestions and corrections. The research of C.-W. Shu was partially supported by NSF grant DMS-1719410.

References

[1] C. Hirsch, Numerical Computation of Iternal and External flows, 2nd ed., Elsevier, 2007.
[2] P. Kaps, S.W.H. Poon, T.D. Bui, Rosenbrock methods for stiff ODEs: a comparison of Richardson extrapolation and embedding technique, Computing 34 (1985) 17–40.
[3] J. Franke, W. Frank, Application of generalized Richardson extrapolation to the computation of the flow across an asymmetric street intersection, J. Wind Eng. Ind. Aerodyn. 96 (2008) 1616–1628. 4th International Symposium on Computational Wind Engineering (CWE2006).

[4] L.F. Richardson, The approximate arithmetical solution by finite differences of physical problems involving differential equations, with an application to the stresses in a masonry dam, Philos. Trans. R. Soc. Lond. Ser. A, Contain. Pap. Math. Phys. Character 210 (1910) 307–357.
[5] L.F. Richardson, J.A. Gaunt, The deferred approach to the limit. Part I. Single lattice. Part II. Interpenetrating lattices, Philos. Trans. R. Soc. Lond. Ser. A Contain. Pap. Math. Phys. Character 226 (1927) 299–361.
[6] P.J. Roache, P.M. Knupp, Completed Richardson extrapolation, Commun. Numer. Methods Eng. 9 (1993) 365–374.
[7] C. Marchi, F.F. Giacomini, C.D. Santiago, Repeated Richardson extrapolation to reduce the field discretization error in computational fluid dynamics, Numer. Heat Transf. Part B 70 (2016) 340–353.
[8] J. Martn-Vaquero, B. Kleefeld, Extrapolated stabilized explicit Runge–Kutta methods, J. Comput. Phys. 326 (2016) 141–155.
[9] P. Amore, J.P. Boyd, F.M. Fernndez, B. Rsler, High order eigenvalues for the Helmholtz equation in complicated non-tensor domains through Richardson extrapolation of second order finite differences, J. Comput. Phys. 312 (2016) 252–271.
[10] A. Dang, H. Kehtarnavaz, D. Coats, The use of Richardson extrapolation in PNs solutions of rocket nozzle flow, in: Proceedings of the 25th Joint Propulsion Conference, American Institute of Aeronautics and Astronautics, Monterey, Califrnia, 1989.
[11] C.H. Marchi, M.A. Martins, L.A. Novak, L.K. Araki, M.A.V. Pinto, S. de F.T. Gonalves, D.F. Moro, I.d.S. Freitas, Polynomial interpolation with repeated Richardson extrapolation to reduce discretization error in CFD, Appl. Math. Model. 40 (2016) 8872–8885.
[12] C.W. Shu, Essentially non-oscillatory and weighted essentially non-oscillatory schemes for hyperbolic conservation laws, in: A. Quarteroni (Ed.), Advanced Numerical Approximation of Nonlinear Hyperbolic Equations, Springer, Berlin, 1998, pp. 325–432.
[13] S. Gottlieb, D. Gottlieb, C.W. Shu, Recovering high-order accuracy in WENO computations of steady-state hyperbolic systems, J. Sci. Comput. 28 (2006) 307–318.
[14] C.H. Marchi, L.A. Novak, C.D. Santiago, A.P.d.S. Vargas, Highly accurate numerical solutions with repeated Richardson extrapolation for 2D Laplace equation, Appl. Math. Model. 37 (2013) 7386–7397.
[15] C.H. Marchi, E.M. Germer, Effect of ten CFD numerical schemes on repeated Richardson extrapolation (RRE), J. Appl. Comput. Math. 2 (2013) 1–9.
[16] R. Borges, M. Carmona, B. Costa, W.S. Don, An improved weighted essentially non-oscillatory scheme for hyperbolic conservation laws, J. Comput. Phys. 227 (2008) 3191–3211.
[17] J.D. Anderson, Modern Compressible Flow: With Historical Perspective, 3rd ed., McGraw–Hill, New York, 2003.
[18] S. Tan, C.W. Shu, Inverse Lax–Wendroff procedure for numerical boundary conditions of conservation laws, J. Comput. Phys. 229 (2010) 8144–8166.
[19] S. Tan, C. Wang, C.-W. Shu, J. Ning, Efficient implementation of high order inverse Lax–Wendroff boundary treatment for conservation laws, J. Comput. Phys. 231 (2012) 2510–2527.
[20] Standard for Verification and Validation in Computational Fluid Dynamics and Heat Transfer, American Society of Mechanical Engineers, New York, 2009. https://www.asme.org/codes-standards/find-codes-standards/v-v-20-standard-verification-validation-computational-fluid-dynamics-heat-transfer#ASME-digital-books.
[21] C.H. Marchi, A.F.C.d. Silva, Unidimensional numerical solution error estimation for convergent apparent order, Numer. Heat Transf. 42 (2002) 167–188.
[22] P.J. Roache, Fundamentals of Verification and Validation, Hermosa Publishers, New Mexico, 2009.
[23] W.-S. Don, R. Borges, Accuracy of the weighted essentially non-oscillatory conservative finite difference schemes, J. Comput. Phys. 250 (2013) 347–372.
[24] J. Zhu, C.W. Shu, Numerical study on the convergence to steady state solutions of a new class of high order WENO schemes, J. Comput. Phys. 349 (2017) 80–96.